

Tailoring a two-dimensional electron gas at the LaAlO₃/SrTiO₃ (001) interface by epitaxial strain

C. W. Bark^a, D. A. Felker^b, Y. Wang^c, Y. Zhang^d, H. W. Jang^a, C. M. Folkman^a, J. W. Park^a, S. H. Baek^a, X. Q. Pan^d, E. Y. Tsybal^c, M. S. Rzchowski^b, C. B. Eom^{a,1}

^aDepartment of Materials Science and Engineering, University of Wisconsin, Madison, WI 53706, USA

^bDepartment of Physics, University of Wisconsin, Madison, WI 53706, USA

^cDepartment of Physics and Astronomy, Nebraska Center for Materials and Nanoscience, University of Nebraska, Lincoln, NE 68588, USA

^dDepartment of Materials Science and Engineering, University of Michigan, Ann Arbor, MI 48109, USA

¹To whom correspondence should be addressed. E-mail: eom@engr.wisc.edu.

Corresponding author: Chang-Beom Eom,
2164 ECB, 1550 Engineering Drive, Madison, WI 53706
Tel: 608/263-6305, Fax: 608/263-9017, E-mail: eom@engr.wisc.edu

Abstract

Recently a metallic state was discovered at the interface between insulating oxides, most notably LaAlO_3 and SrTiO_3 . Properties of this two-dimensional electron gas (2DEG) have attracted significant interest due to its potential applications in nanoelectronics. Control over this carrier density and mobility of the 2DEG is essential for applications of these novel systems, and may be achieved by epitaxial strain. However, despite the rich nature of strain effects on oxide materials properties, such as ferroelectricity, magnetism, and superconductivity, the relationship between the strain and electrical properties of the 2DEG at the $\text{LaAlO}_3/\text{SrTiO}_3$ heterointerface remains largely unexplored. Here, we use different lattice constant single crystal substrates to produce $\text{LaAlO}_3/\text{SrTiO}_3$ interfaces with controlled levels of biaxial epitaxial strain. We have found that tensile strained SrTiO_3 destroys the conducting 2DEG, while compressively strained SrTiO_3 retains the 2DEG, but with a carrier concentration reduced in comparison to the unstrained $\text{LaAlO}_3/\text{SrTiO}_3$ interface. We have also found that the critical LaAlO_3 overlayer thickness for 2DEG formation increases with SrTiO_3 compressive strain. Our first-principles calculations suggest that a strain-induced electric polarization in the SrTiO_3 layer is responsible for this behavior. It is directed away from the interface and hence creates a negative polarization charge opposing that of the polar LaAlO_3 layer. This both increases the critical thickness of the LaAlO_3 layer, and reduces carrier concentration above the critical thickness, in agreement with our experimental results. Our findings suggest that epitaxial strain can be used to tailor 2DEGs properties of the $\text{LaAlO}_3/\text{SrTiO}_3$ heterointerface.

\body

Introduction

Strains have previously been used to engineer and enhance numerous properties of materials. For example, increased mobility in semiconductors (1,2), and increased transition temperature in ferroelectric materials (3,4,5,6) and superconductors (7) have been observed. A recently discovered two-dimensional electron gas (2DEG) at the $\text{LaAlO}_3/\text{SrTiO}_3$ interface (8,9) has attracted great interest due to its novel application to nanoscale oxide devices (10). So far, most studies of 2DEGs at oxide interfaces were performed using TiO_2 -terminated SrTiO_3 bulk single crystal substrates. Thus, despite the rich nature of strain effects on oxide materials properties, the relationship between the strain and electrical properties of the 2DEG at the $\text{LaAlO}_3/\text{SrTiO}_3$ heterointerface remains largely unexplored.

The importance of strain effects comes from the fact that integrating 2DEGs to other functional devices or substrates always involves strain. Therefore, it is desirable to know the effect of the strain on 2DEG at the $\text{LaAlO}_3/\text{SrTiO}_3$ interface. In addition, by changing strain we might be able to obtain novel functional properties. For example, strain can induce an electric polarization in otherwise non-polar SrTiO_3 (11). It has been predicted that polarization can be used to control 2DEG properties at oxide heterointerfaces (12,13). Thus by using the relation between the polarization and the strain, we could engineer 2DEG behavior.

To address these outstanding issues, we explore the effect of epitaxial strain on conductive properties of $\text{LaAlO}_3/\text{SrTiO}_3$ interface. We create the 2DEG interface on strained single-crystal (001) SrTiO_3 templates grown on perovskite oxide substrates with various lattice mismatch. Pseudomorphic growth of the $\text{LaAlO}_3/\text{SrTiO}_3$ bilayer produces a continuously strained system, including the interface at which the 2DEG resides. This allows us to add a new degree of freedom in the $\text{LaAlO}_3/\text{SrTiO}_3$ system and investigate the strain effect on its transport properties. We demonstrate that tensile strain makes the interface insulating, while compressive strain makes the interface metallic and allows modulating the critical thickness of LaAlO_3 and conductivity of the 2DEG.

Sample growth

$\text{LaAlO}_3/\text{SrTiO}_3$ thin films heterostructures were grown on various single crystal substrates using pulsed-laser deposition (PLD) with *in-situ* high pressure reflection high-energy electron diffraction (RHEED) (14). Figure 1A shows the schematic of the thin film heterostructure. Table 1 shows substrates that were used in this study to vary the SrTiO_3 strain state from biaxial compressive to biaxial tensile in the plane. As shown in figure 1, (001) SrTiO_3 thin films were grown on (110) NdGaO_3 (NGO), (001) $(\text{LaAlO}_3)_{0.3}-(\text{Sr}_2\text{AlTaO}_3)_{0.7}$ LSAT, (110) DyScO_3 (DSO) and (110) GdScO_3 (GSO) substrates. The varying lattice parameters result in an average biaxial strain ranging from -1.21% (compressive) to +1.59% (tensile) in a fully commensurate SrTiO_3 deposited film. All grown single-crystal (001) SrTiO_3 templates were fully coherent with the substrates. (001) SrTiO_3 films were also grown on (001) silicon substrates using Molecular Beam Epitaxy. Thickness of these quasi-single-crystal (001) SrTiO_3 templates on silicon was 100 nm, and the films were almost fully relaxed. The measured SrTiO_3 lattice parameters on Si correspond to an average biaxial strain of 0.15% (15,16). The bi-axial strain state and lattice parameters of the strained (001) SrTiO_3 templates are

summarized in Table 1. The full width at half maximum (FWHM) values of 002 rocking curves for the strained SrTiO₃ template are much narrower than that of the bulk SrTiO₃ single crystal (17). The single-crystal (001) SrTiO₃ templates were also etched using buffered HF solution to maintain Ti-termination after the growth. The atomic percent of Sr, Ti, O in the films were determined with wavelength dispersive x-ray spectroscopy (WDS). The chemical ratio of grown templates was the same as the one of SrTiO₃ bulk single crystal within an error range. This confirms that the quality of SrTiO₃ templates is comparable with the bulk single crystal SrTiO₃ substrate, therefore, we rule out any extrinsic effects in our experiments.

LaAlO₃ overlayers were deposited using PLD on these various strain Ti-terminated single crystal SrTiO₃ templates. RHEED intensity oscillations of the specular spots show layer-by-layer growth mode as observed for LaAlO₃ films on SrTiO₃ single crystal substrates as shown in figure 1B. High resolution TEM cross-sectional analysis in figure 1C shows the LaAlO₃/SrTiO₃ film on LSAT with high crystalline quality and atomically sharp interface. In all strain states, surfaces of LaAlO₃ and SrTiO₃ films were atomically smooth with single unit cell high steps measured by atomic force microscopy (AFM), as seen in figure 1D. As a result, we confirmed that all biaxial strained heterostructures in this report were atomically controlled and grown epitaxially. More details about growth are described in ref. (11) and *Materials and Methods*.

Results and Discussion

It is known experimentally that a conducting 2DEG forms at the LaAlO₃ / bulk SrTiO₃ interface only after the LaAlO₃ overlayer thickness exceeds a critical value of 4 unit cells (18). We have found that this critical thickness depends on the strain of the system. We determined this by measuring the conductivity of strained LaAlO₃/SrTiO₃ bilayers for different thickness of the LaAlO₃ layer. As shown in Fig. 1, LaAlO₃ overlayer thickness was changed from 0 to 30 unit cells while the thickness of SrTiO₃ template on NGO, LSAT, DSO, GSO substrates was fixed at 50 unit cells. We also checked the critical thickness of LaAlO₃ on Ti-terminated (001) SrTiO₃ bulk single crystal and on quasi-single-crystal (001) SrTiO₃ templates on silicon (19) as a reference.

In case of the two samples with un-strained SrTiO₃ layers (LaAlO₃ on bulk single crystal SrTiO₃ substrate and LaAlO₃ on relaxed SrTiO₃ templates on silicon), the critical thickness was in agreement with that previously reported, i.e. 4 unit cells. However, in the compressive strain states, (SrTiO₃ templates on LSAT and NGO), the critical thickness of LaAlO₃ increased to 10 unit cells and 15 unit cells, respectively, as

shown in Fig. 2A. In all the cases, the conductivity saturated above the critical thickness of the LaAlO₃ overlayer. However, unlike the non-strained state, the conductivity versus thickness of LaAlO₃ had a gradual rather than an abrupt change at the critical thickness. For instance, in case of LaAlO₃/SrTiO₃/LSAT measurable conductivity was detected at 10 unit cells LaAlO₃ thickness, but it did not saturate until 20 unit cells. There is however a clear trend of increasing LaAlO₃ critical thickness with increasing compressive biaxial in-plane strain.

Figure 2B shows the carrier concentration at each strain state above the critical thickness of LaAlO₃. Similar to the critical thickness of LaAlO₃ layer, we find nearly the same carrier concentration at both near-zero strain states, LaAlO₃ on SrTiO₃ bulk single crystal and LaAlO₃ on quasi-single crystal (001) SrTiO₃ template on Silicon. The saturation carrier concentration (above the critical thickness) decreased with increasing compressive strain. Although LaAlO₃/SrTiO₃ interfaces on DSO and GSO were grown and treated in the same manner, the interfaces were not conducting within our measurement limit at any thickness of LaAlO₃ overlayer in these tensile-strained films.

Our experimental results indicate that tensile-strained SrTiO₃ destroys the conducting interfacial 2DEG, while compressive-strained SrTiO₃ preserves the 2DEG, but with decreased interfacial carrier concentration. The maximum carrier concentration at the SrTiO₃ unstrained state suggests that it is the strain-dependence of SrTiO₃ properties that control the 2DEG. It has been predicted theoretically that free-standing biaxially strained SrTiO₃ under electrical short-circuit boundary conditions can develop an electric polarization (20,21). Compressive strain is predicted to produce an [001] (out-of-plane) polarization, and tensile strain to produce a [110] (in-plane) polarization. Experimental evidence suggests a more complex picture, with many strain-states resulting in a relaxor behavior at room temperature (11,,22) without a stable switchable polarization.

However we expect the strain-induced STO properties to be altered by the LaAlO₃ overlayer. Observations from TEM (23,24), synchrotron radiation x-ray scattering (25,26), and tunneling (27), indicate that in strain-free SrTiO₃ a few unit cells near the LaAlO₃ interface have ferroelectric-like structural distortions with local polarization pointing away from the interface, and decreasing in magnitude with distance from the interface (28). Biaxial compressive strain induces a tetragonal distortion along 001, which would enhance this polarization, potentially uniformly polarizing the SrTiO₃ throughout its thickness. (29).

Figure 3 schematically compares the strained and unstrained systems. In the unstrained system positively charged (LaO)⁺ atomic layers and negatively charged

$(\text{AlO}_2)^-$ atomic layers create an average polarization whose positive bound charge resides at the interface, as shown schematically in the left panel of Fig. 3A. This polarization charge is responsible for the intrinsic electric field E_0 in LaAlO_3 (shown by arrow in Fig. 3A) resulting in an electric potential difference between the LaAlO_3 surface and the $\text{LaAlO}_3/\text{SrTiO}_3$ interface that increases with LaAlO_3 layer thickness. Above the LaAlO_3 critical thickness, charge is transferred to the $\text{LaAlO}_3/\text{SrTiO}_3$ interface (shown by a blue filling) to avoid this polarization catastrophe.

The compressively strained SrTiO_3 layer contains polar displacements of the Ti^{4+} ions with respect to the O^{2-} ions, shown in Fig. 3B for the case of uniform polarization. These displacements are responsible for a polarization P pointed away from the interface (indicated by an arrow at the bottom of the left panel of Fig. 3B). The polarization orientation is determined by the presence of the LAO layer and is likely not switchable. The polarization produces a negative bound charge at the $\text{LaAlO}_3/\text{SrTiO}_3$ interface (indicated in the left panel of Fig. 3B) that creates an additional electric field in LaAlO_3 equal to P/ϵ , where ϵ is the dielectric constant of LaAlO_3 , that opposes the intrinsic electric field E_0 . The presence of polarization in the compressively strained SrTiO_3 layer reduces the total electric field in LaAlO_3 and hence enhances the critical thickness necessary to create a 2DEG at the $\text{LaAlO}_3/\text{SrTiO}_3$ interface due to the polarization catastrophe effect. Above this critical thickness, the mobile interfacial carrier concentration would be reduced by the interfacial bound charge (12,13).

In order to quantify these effects we have completed first-principles calculations of the $\text{LaAlO}_3/\text{SrTiO}_3$ bilayer under various strain states based on density functional theory (DFT), as described in *Materials and Methods*. Fig. 4 shows calculated ionic displacements for the unstrained and 1.2% compressively strained $(\text{LaAlO}_3)_3/(\text{SrTiO}_3)_5$ structures. It is seen that in the unstrained case polar Ti-O displacements in the SrTiO_3 layer are very small, consistent with the previous calculations (33). The in-plane 1.2% compressive strain produces sizable ionic displacements, polarizing the SrTiO_3 layer. The calculation predicts that the induced polarization is oriented away from the interface and is not switchable. The magnitude of the polarization is $P \approx 0.18 \text{ C/m}^2$, as found from the known polar displacements in the strained SrTiO_3 layer using the Berry phase method (30,31).

The critical thickness t_c in the presence of a STO polarization can be estimated as follows:

$$t_c = \delta\mathcal{E}/eE \quad (1)$$

where $\delta\mathcal{E} = e\mathcal{E}_g + (\mathcal{E}_{VBM}^{STO} - \mathcal{E}_{VBM}^{LAO})$, \mathcal{E}_g is the band gap of SrTiO_3 , \mathcal{E}_{VBM}^{STO} and \mathcal{E}_{VBM}^{LAO} are

the valence band maxima (VBM) of SrTiO₃ and LaAlO₃ respectively, and E is the electric field in LaAlO₃. The latter is reduced from the intrinsic value of E_0 due to polarization P of SrTiO₃ so that

$$E = E_0 - \frac{P}{\epsilon_{LAO}}, \quad (2)$$

where ϵ_{LAO} is the dielectric constant of LaAlO₃. Due to the reduced electric field in LaAlO₃ in the presence of the SrTiO₃ polarization, the critical thickness (1) is enhanced. The intrinsic electric field E_0 can be estimated from the experimentally measured critical thickness $t_c^0 = 4$ u.c. for the unstrained system. Taking into account the experimental

band gap of STO $\epsilon_g = 3.2$ eV and the CBM offset between SrTiO₃ and LaAlO₃

$\epsilon_{VBM}^{STO} - \epsilon_{VBM}^{LAO} = 0.35$ eV, (32) we find that $\delta\mathcal{E} = 3.55$ eV. Using the relationship

$$\delta\mathcal{E} = eE_0 t_c^0 \quad (3)$$

we obtain that $E_0 \approx 0.23$ V/Å which is consistent with our first-principles calculation predicting $E_0 \approx 0.22$ V/Å and calculations by others (33,34,35). Using Eqs. (1-3) we obtain

$$t_c = \frac{t_c^0}{1 - \frac{P}{\epsilon_{LAO} E_0}}. \quad (4)$$

Using the calculated polarization value $P \approx 0.18$ C/m² for 1.2% compressive strain in the STO layer, and the calculated electric fields in the LaAlO₃ and SrTiO₃ layers in the strained LaAlO₃/SrTiO₃ system, we estimate the dielectric constant of the LaAlO₃ grown on 1.2% compressively strained SrTiO₃ to be $\epsilon_{LAO} \approx 18\epsilon_0$. This value is consistent with that obtained from the induced polarization of 0.34 C/m² in the LaAlO₃ layer, as is estimated from the calculated ionic displacements using the Berry phase method. (We note that the estimated value of the dielectric constant of the unstrained LaAlO₃ is $\epsilon_{LAO} \approx 24\epsilon_0$ which is consistent with the previously found result (36)). Using Eq. (4) and the dielectric constant $\epsilon_{LAO} \approx 18\epsilon_0$ we obtain $t_c \approx 9$ u.c. This value is higher than the critical thickness (4 u.c.) for the unstrained system, and is consistent with the experimental result for the 1.2% strained LaAlO₃/SrTiO₃ structure. It is relevant to the experimental situation where it is expected that the surface polarization charge in LaAlO₃ is screened by adsorbents and the bottom polarization charge in the strained SrTiO₃ is screened by defects. In the structural model used in our DFT calculation the SrTiO₃ polarization is screened by charge transferred to the SrTiO₃ surface.

For the case of tensile strain in the STO layer, our experiments indicate that there is no conducting 2DEG for biaxial tensile strains above 1.1%. Free-standing SrTiO₃ has been predicted at zero temperature to develop an in-plane polarization in the (110) direction under biaxial tensile strain. Experiment suggests that, at room temperature, relaxor behavior, with nanoscale polar regions that can be aligned in an electric field, occurs in many tensile strained SrTiO₃ samples. Stabilization of a uniform in-plane polarization by the LaAlO₃ layer does not seem likely. If such nanoscale regions near to the interface were present in our samples, bound charge at polarization discontinuities between random nanopolar regions would tend to be locally screened by carriers at the 2DEG interface. This would lead to localization of these carriers, preventing us from observing conduction in these samples.

Another aspect is strain in the LaAlO₃ overlayer. The bulk pseudocubic lattice constant of LaAlO₃ is 3.791 Å, so that coherent LaAlO₃ even on unstrained SrTiO₃ has a 3% tensile strain. Growing the bilayer on a GSO substrate results in 4.5% tensile strain in the LaAlO₃ layer. An NGO substrate reduces the LaAlO₃ strain to 1.8% tensile, but for all substrates used the LAO layer is under tensile strain. Our transmission electron microscopy analysis of these samples indicates that the LaAlO₃ layer on SrTiO₃ is fully coherent when grown on LSAT (2% LaAlO₃ tensile strain) and STO, but that growth on DSO (leading to 4% LaAlO₃ tensile strain) results in partial relaxation of the LaAlO₃. Such defect incorporation might alter the conduction properties of the interface. However, the SrTiO₃ layer on Si (grown by MBE) is almost fully relaxed, and the bilayer shows a fully conducting interfacial 2DEG, but with lower mobility. This suggests that such defects do not destroy the 2DEG. Large tensile strain in LaAlO₃ has been predicted (37) to alter the Al-O bond lengths, which could affect the electronic structure.

We have demonstrated that properties of the 2DEG formed at the LaAlO₃/SrTiO₃ interface can be controlled by epitaxial strain. Both the critical thickness of the LaAlO₃ overlayer required to generate the 2DEG and the carrier concentration of the 2DEG depend on the strain of the SrTiO₃ layer. Compressive strain increases the critical thickness and decreases the saturated carrier concentration. Our DFT calculations indicate that a strain-induced polarization stabilized by the LaAlO₃ overlayer is responsible for these changes. Changes in critical thickness and carrier concentration estimated from the DFT calculations are in agreement with the experimental data.

The dependence of 2DEG properties at the LaAlO₃/SrTiO₃ interface on the strain state opens a new correlation between strain-induced polarization and the

electrical properties of oxide interfaces. We believe that such strain engineering can be very useful for oxide 2DEG device applications, and the relation between strain and 2DEG properties provides a new tool in the manipulation of oxide interfacial 2DEGs.

Materials and Methods

Epitaxial LaAlO₃ and STO thin films were grown on (001) LSAT, (110) NdGaO₃, (110) GdScO₃, and (110) DyScO₃ substrates by PLD. To grow heterostructures by PLD, substrates were attached to a resistive heater and positioned 5.0~6.0 cm from the target. A KrF excimer laser (248 nm) beam was focused on a stoichiometric LaAlO₃ and SrTiO₃ single crystal target to an energy density of 2.0~2.5 J/cm² and pulsed at 3~5 Hz. SrTiO₃ templates were grown at substrate temperatures ranging from 650 to 850 °C and oxygen pressures of 10-100 mTorr. Before deposition, low miscut (<0.05°) LSAT, NGO, DSO, GSO substrates were treated by a modified buffered HF etch and annealed in oxygen at 1000~1100°C for 2~12 hours to create atomically smooth surfaces with unit cell step. The PLD system is equipped with high-pressure RHEED, which enabled atomic layer controlled growth and *in situ* monitoring during the growth. SrTiO₃ templates were etched using buffered HF acid for 30~90 seconds to maintain Ti-termination after growth SrTiO₃ layer. LaAlO₃ films were grown at 550 °C at oxygen pressures of 10⁻³ mbar and cooled down to room temperature at the same oxygen pressure.

The three-dimensional strain state of the films was determined using high-resolution four-circle x-ray diffraction (Bruker D8 advance). The microstructure and interfacial structure of the samples were characterized by cross-sectional transmission electron microscopy (TEM). Surface of films were imaged by AFM (Veeco).

After the growth, Al contacts were made by wire bonding near the four corners of the sample for van der Pauw electrical characterization. A Keithley 2700 sourcemeter combined with a 2400 switch matrix multimeter was used for the van der Pauw measurements of conductance and carrier concentration. The sheet resistance was calculated by fitting slopes to the four point IV curves measured between the four combinations of contacts. The nominal sheet carrier concentration was determined from the Hall coefficient as $n_{2D} = -t/R_H e$ where t is the film thickness, R_H is the Hall coefficient, and e is the charge of an electron. The mobility was determined from the sheet resistance R_{\square} and sheet carrier concentration n_{2D} as $\mu = 1/en_{2D}R_{\square}$.

Density functional calculations were performed within the local density approximation (LDA) using the VASP method (38,39), similar to the calculations

performed previously (40). We considered a LaO/TiO₂-interfaced (LaAlO₃)_n/(SrTiO₃)_m bilayer (where n and m are the numbers of unit cells of LaAlO₃ and SrTiO₃ respectively), as a model system. The LaAlO₃/SrTiO₃ bilayer was placed in a LaAlO₃/SrTiO₃/vacuum/SrTiO₃/LaAlO₃/vacuum supercell, where the doubled bilayer was used to avoid an unphysical electric field in vacuum which otherwise would occur due to the potential step within the LaAlO₃ layer and periodic boundary conditions of the supercell calculations. The in-plane lattice constant of the unstrained superlattice was fixed to the calculated bulk lattice constant of SrTiO₃, *i.e.* $a = 3.871 \text{ \AA}$. For the strained systems the in-plane lattice constant was constrained to be by a certain percentage smaller than the bulk one. To reduce the effect of the SrTiO₃ surface on atomic structure and ionic displacements within the SrTiO₃ layer we used a boundary condition according to which the atomic positions within one unit cell on the SrTiO₃ surface were fixed to be the same as in the respectively strained bulk SrTiO₃. The latter were computed separately for the unstrained and strained bulk SrTiO₃. All the other atoms in the superlattices were relaxed.

Acknowledgements

This work was supported by the National Science Foundation under Grant No. DMR-0906443, and a David and Lucile Packard Fellowship (C.B.E.). The research at University of Nebraska was supported by the Materials Research Science and Engineering Center (NSF Grant No. DMR-0820521) and the Nebraska Research Initiative. The work at the University of Michigan was supported by DMR-0907191, DoE/BES DE-FG02-07ER46416, and NSF/DMR-0723032.

References

- 1 Min Chu, Yongke Sun, Umamaheswari Aghoram, Scott E. Thompson (2009) Strain: A Solution for Higher Carrier Mobility in Nanoscale MOSFETs. *Annu. Rev. Mater. Res.* 39: 203-229
- 2 Welser J, Hoyt JL, Gibbons JF. (1994) Electron mobility enhancement in strained-Si n-type metal-oxide-semiconductor field-effect transistors. *IEEE Electron. Device Lett.* 15:100–2
- 3 Choi KJ et al. (2004) Enhancement of Ferroelectricity in Strained BaTiO₃ Thin Films. *Science* 306:1005-1009.
- 4 Warusawithana MP et al. (2009) A Ferroelectric Oxide Made Directly on Silicon.

-
- Science 324:367-370.
- 5 Reiner JW et al. (2010) Crystalline Oxides on Silicon. *Adv. Mater.* 22:2919-2938.
 - 6 Woerdenweber R, Hollmann E, Kutzner R, Schubert J (2007) Induced ferroelectricity in strained epitaxial SrTiO₃ films on various substrates. *J. Appl. Phys.* 102:044119.
 - 7 Gozar A, Logvenov G, Fitting Kourkoutis L, Bollinger AT, Giannuzzi LA, Muller DA and Bozovic I (2008) High-temperature interface superconductivity between metallic and insulating copper oxides. *Nature* 455:782-785
 - 8 Ohtomo A, Hwang HY (2004) A high-mobility electron gas at the LaAlO₃/SrTiO₃ heterointerface. *Nature* 427:423-426.
 - 9 Ohtomo A, Muller DA, Grazul JL, Hwang HY (2002) Artificial charge-modulation in atomic-scale perovskite titanate superlattices. *Nature* 419:378-380.
 - 10 Cen C, Thiel S, Mannhart J, Levy J (2009) Oxide Nanoelectronics on Demand. *Science* 323:1026-1030.
 - 11 Jang HW et al. (2010) Ferroelectricity in Strain-Free SrTiO₃ Thin Films. *Phys. Rev. Lett.* 104: 169601
 - 12 Niranjana MK, Wang Y, Jaswal SS, Tsymbal EY (2009) Prediction of a Switchable Two-Dimensional Electron Gas at Ferroelectric Oxide Interfaces. *Phys. Rev. Lett.* 103:016804.
 - 13 Wang Y, Niranjana MK, Jaswal SS, Tsymbal EY (2009) First-principles studies of a two-dimensional electron gas at the interface in ferroelectric oxide heterostructures. *Phys. Rev. B* 80:165130.
 - 14 Rijnders GJHM, Koster G, Blank DHA, Rogalla H (1997) In situ monitoring during pulsed laser deposition of complex oxides using reflection high energy electron diffraction under high oxygen pressure. *Appl. Phys. Lett.* 70:1888.
 - 15 Park JW, Baek SH, Bark CW, Biegalski MD, Eom CB (2009) Quasi-single-crystal (001) SrTiO₃ templates on Si. *Appl. Phys. Lett.* 95:061902.
 - 16 Lee S et al. (2010) Template engineering of Co-doped BaFe₂As₂ single-crystal thin films. *Nat Mater* 9:397-402.
 - 17 Schlom DG, Chen L, Pan X, Schmehl A, Zurbuchen MA (2008) A Thin Film Approach to Engineering Functionality into Oxides. *Journal of the American Ceramic Society* 91:2429-2454.
 - 18 Thiel S, Hammerl G, Schmehl A, Schneider CW, Mannhart J (2006) Tunable Quasi-Two-Dimensional Electron Gases in Oxide Heterostructures. *Science* 313:1942-1945.
 - 19 Park et al, *Nature Communications* (in press)

-
- 20 A Antons, JB Neaton, KM Rabe, D Vanderbilt (2005), Tunability of the dielectric response of epitaxially strained SrTiO₃ from first principles. *Phys Rev B* 71: 024102.
 - 21 Sheng G, Li YL, Zhang JX, Choudhury S, Jia QX, Gopalan V, Schlom DG, Liu ZK, Chen LQ (2010) A modified Landau-Devonshire thermodynamic potential for strontium titanate. *Appl. Phys. Lett.* 96:232902.
 - 22 Biegalski MD, Jia Y, Schlom DG, Trolier-McKinstry S, Streiffer SK, Sherman V, Uecker R, Reiche P (2006) Relaxor ferroelectricity in strained epitaxial SrTiO₃ thin films on DyScO₃ substrates. *Appl. Phys. Lett.* 88:192907
 - 23 Maurice J et al. (2006) Electronic conductivity and structural distortion at the interface between insulators SrTiO₃ and LaAlO₃. *Physica status solidi (a)* 203:2209-2214.
 - 24 Jia CL et al. (2009) Oxygen octahedron reconstruction in the SrTiO₃ / LaAlO₃ heterointerfaces investigated using aberration-corrected ultrahigh-resolution transmission electron microscopy. *Phys. Rev. B* 79:081405.
 - 25 Vonk V et al. (2007) Interface structure of SrTiO₃ /LaAlO₃ at elevated temperatures studied in situ by synchrotron x rays. *Phys. Rev. B* 75:235417.
 - 26 Willmott PR et al. (2007) Structural Basis for the Conducting Interface between LaAlO₃ and SrTiO₃. *Phys. Rev. Lett.* 99:155502.
 - 27 Singh-Bhalla G et al. (2010) Built-in and induced polarization across LaAlO₃/SrTiO₃ heterojunctions, arXiv:1005.4257v1, Nature Physics accepted.
 - 28 Haeni JH et al. (2004) Room-temperature ferroelectricity in strained SrTiO₃. *Nature* 430:758-761.
 - 29 Kamiya T and Kawasaki M (2008) ZnO-Based Semiconductors as Building Blocks for Active Devices. *MRS Bulletin* 33:1061
 - 30 R. Resta (1992) Theory of the electric polarization in crystals, *Ferroelectrics* 36:51.
 - 31 King-Smith RD, Vanderbilt D (1993) Theory of polarization of crystalline solids. *Phys. Rev. B* 47:1651.
 - 32 Segal Y, Ngai JH, Reiner JW, Walker FJ, Ahn CH (2009) X-ray photoemission studies of the metal-insulator transition in LaAlO₃/SrTiO₃ structures grown by molecular beam epitaxy. *Phys. Rev. B* 80:241107.
 - 33 Pentcheva R, Pickett WE (2009) Avoiding the Polarization Catastrophe in LaAlO₃ Overlayers on SrTiO₃(001) through Polar Distortion. *Phys. Rev. Lett.* 102:107602.
 - 34 Chen H, Kolpak AM, Ismail-Beigi S (2009) Fundamental asymmetry in interfacial electronic reconstruction between insulating oxides: An ab initio study. *Phys. Rev.*

-
- B 79:161402.
- 35 Son W, Cho E, Lee B, Lee J, Han S (2009) Density and spatial distribution of charge carriers in the intrinsic n -type LaAlO₃/SrTiO₃ interface. Phys. Rev. B 79:245411.
 - 36 Lee J, Demkov AA (2008) Charge origin and localization at the n -type SrTiO₃/LaAlO₃ interface. Phys. Rev. B 78:193104.
 - 37 Hatt Alison J, Spaldin Nicola A (2010) Structural phases of strained LaAlO₃ driven by octahedral tilt instabilities. arXiv 0808.3792v2
 - 38 Kresse G, Furthmüller J (1996) Efficient iterative schemes for ab initio total-energy calculations using a plane-wave basis set. Phys. Rev. B 54:11169.
 - 39 Kresse G, Furthmüller J (1996) Efficiency of ab-initio total energy calculations for metals and semiconductors using a plane-wave basis set. Computational Materials Science 6:15-50.
 - 40 Janicka K, Velez J, Tsymbal E (2009) Quantum Nature of Two-Dimensional Electron Gas Confinement at LaAlO₃/SrTiO₃ Interfaces. Phys. Rev. Lett. 102:106803.

Figure Legends

Figure 1. Structural characterization of hetero structures. (A) Schematic diagram of grown structures. Thickness of LaAlO_3 layer was varied from 1 to 30 unit cells on STO on LSAT, NGO, Si, DSO, GSO substrate, (B) RHEED intensity oscillations for the growth of LAO and STO on LSAT substrate. The insets show the RHEED pattern at the end of the LAO and STO growth. (C) High-resolution transmission electron microscopy image of LAO on STO on LSAT. Clear intensity differences between separate LaAlO_3 and SrTiO_3 layers in both cases and images showing distinctly the individual La and Sr atoms. (D) AFM images of LAO on STO on DyScO_3 , substrates.

Figure 2. Effect of strain on 2DEG. (A) Critical thickness of LaAlO_3 under bi-axial strain While others samples had 50 unit cell-thick SrTiO_3 layer, LAO/STO/Si had 100nm-thick STO to get nominally unstrained STO layer on silicon. Conductivity verses thickness of LaAlO_3 in LAO/STO interface on various substrates was represented in inset. (B) Sheet resistance at LAO/STO interface under bi-axial strain. Sheet resistances in tensile strain state were above our measurement limit

Figure 3. Calculated atomic structure of unstrained (A) and compressively strained (B) $\text{LaAlO}_3(3\text{u.c.})/\text{SrTiO}_3$ system. In figure B Ti-O and Sr-O displacements are amplified by a factor of eight as compared to the calculated results for visual comprehension. The left and right panels show schematically the 2DEG formation and the effect of the polarization P in the strained SrTiO_3 on the 2DEG as described in text.

Figure 4. B (Ti, Al) cite atom – oxygen (O) atom displacements in the unstrained (squares) and 1.2% compressively strained (circles) $(\text{LaAlO}_3)_3/(\text{SrTiO}_3)_5$ structure.

Table Legend

Table 1. Results from high-resolution x-ray diffraction measurements on the films at room temperature are given. The in-plane (a) and out-of-plane (c) lattice

constants and lattice mismatch between the SrTiO₃ films and single crystal substrates on average of two orthogonal directions. The a- and c-lattice parameters of single-crystalline SrTiO₃ are 3.905Å. All SrTiO₃ templates were fully coherent except STO/Si (12). (002), (101) of SrTiO₃ and cubic substrates, LSAT, Silicon (200)_{pseudo-cubic} of (101)_{pseudo-cubic} of orthorombic substrate, GdScO₃ and DyScO₃, NdGdO₃ were observed to determined in-plane and out-of-plane lattice parameters.

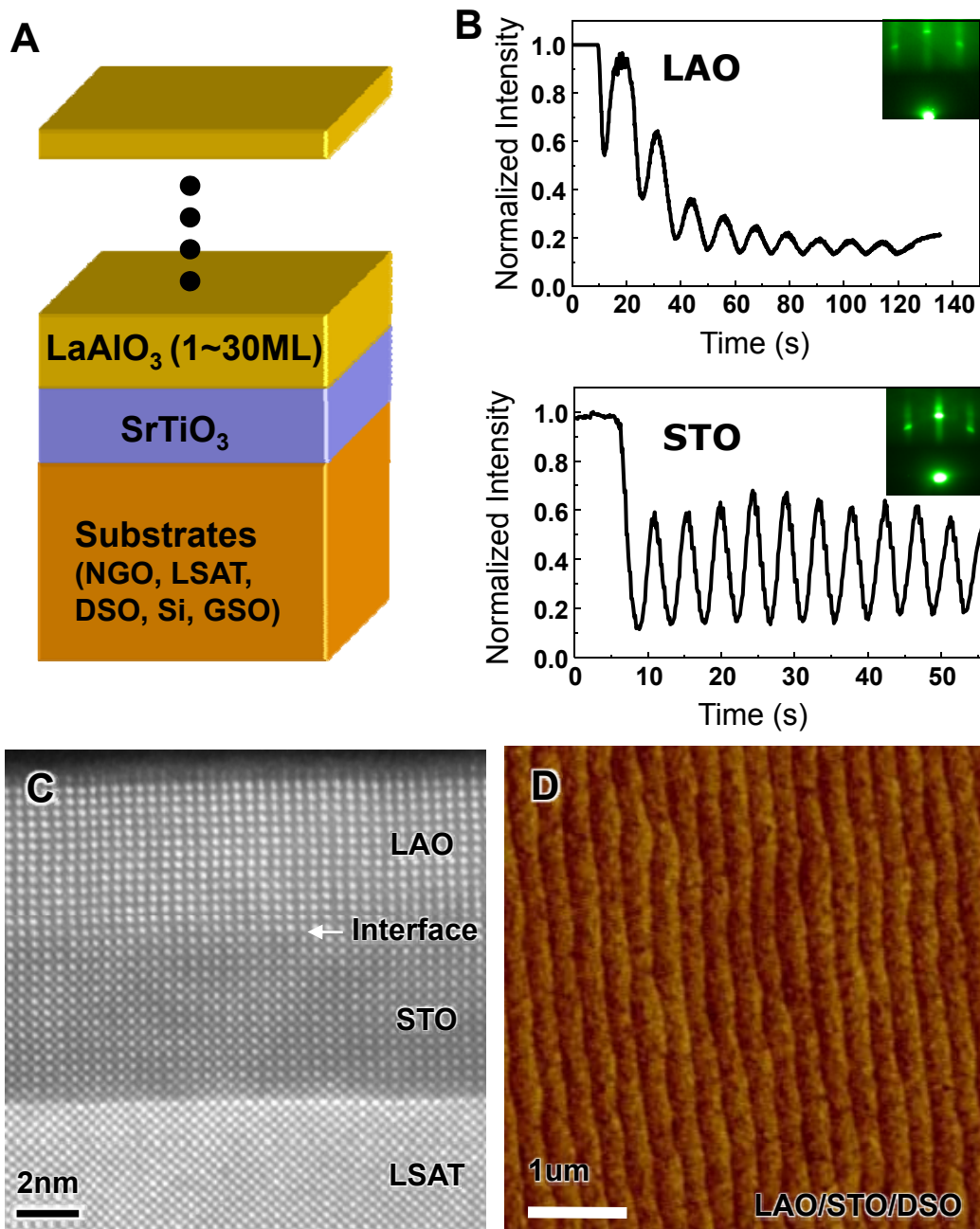


Figure 1, C.W. Bark et al,

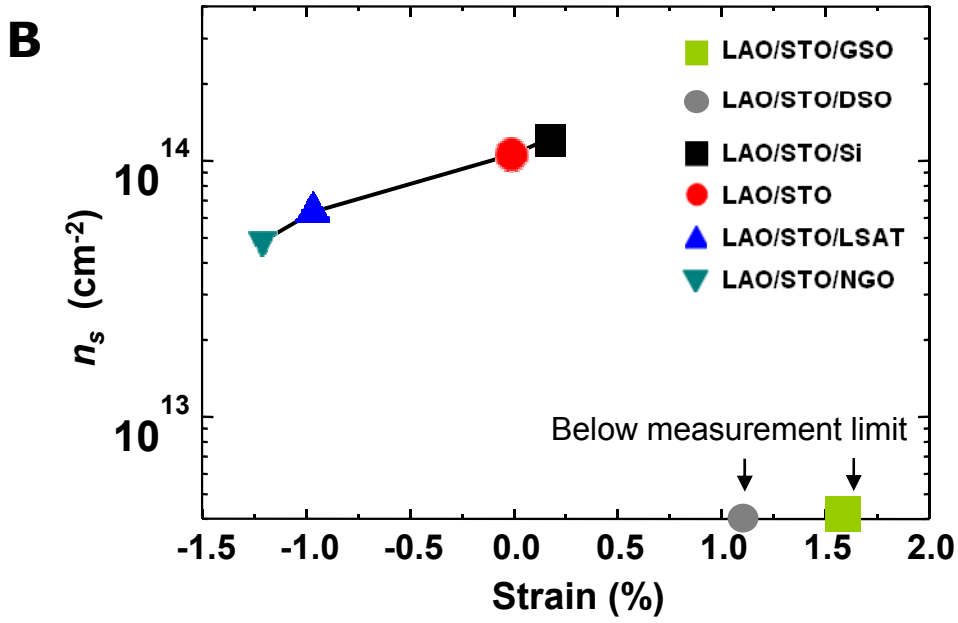
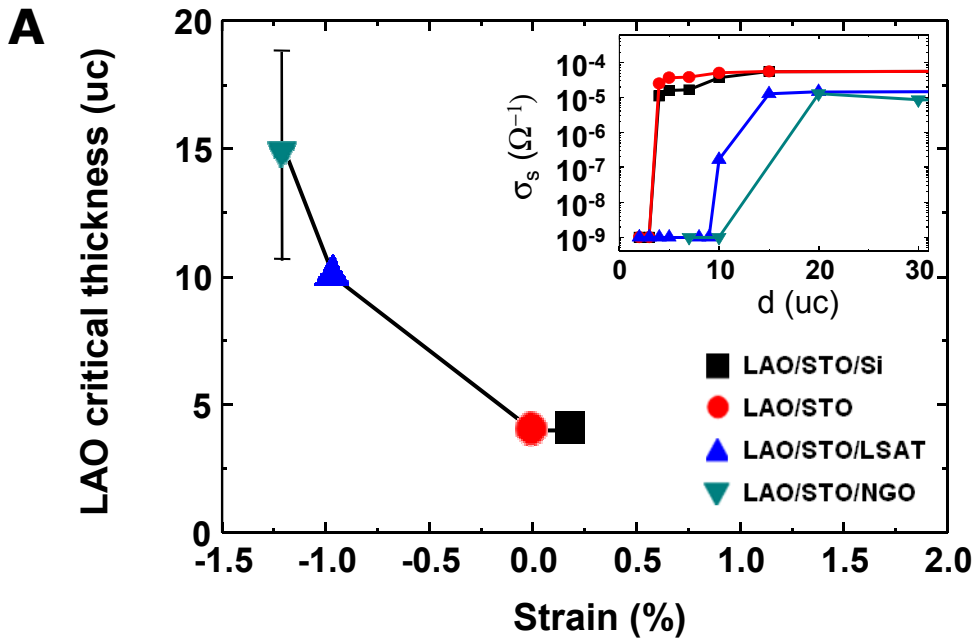


Figure 2, C.W. Bark et al

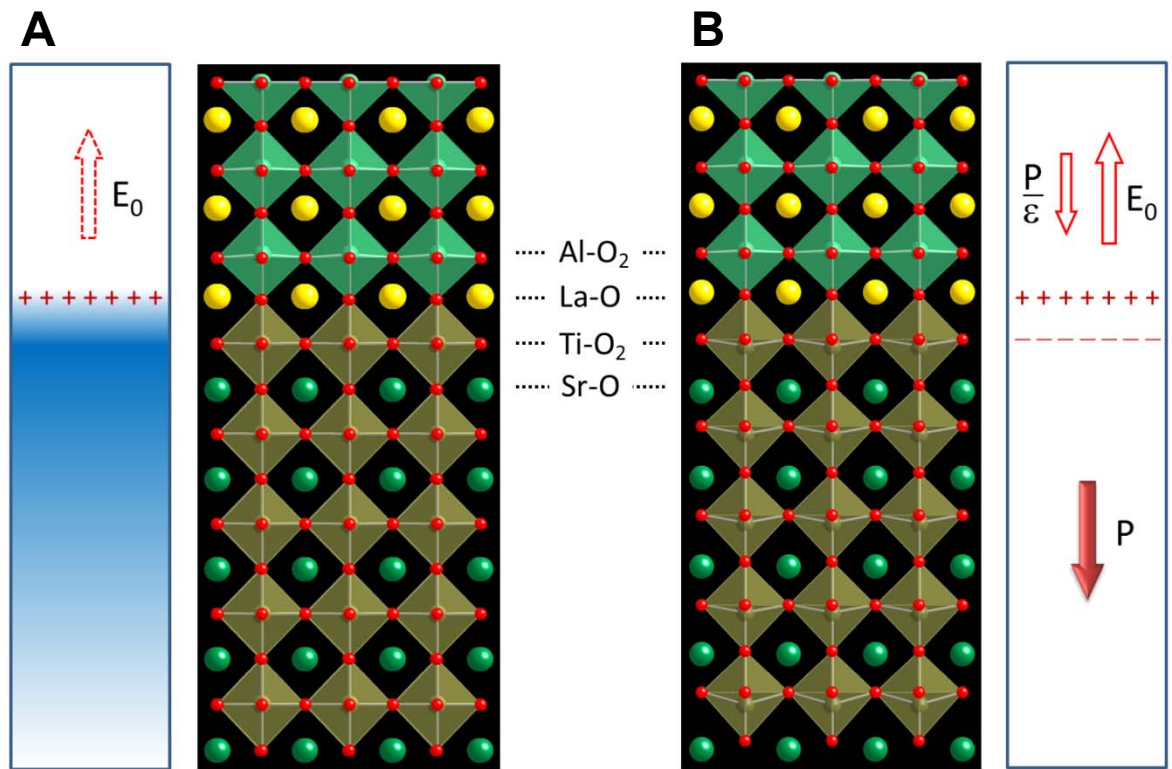


Figure 3, C.W. Bark et al

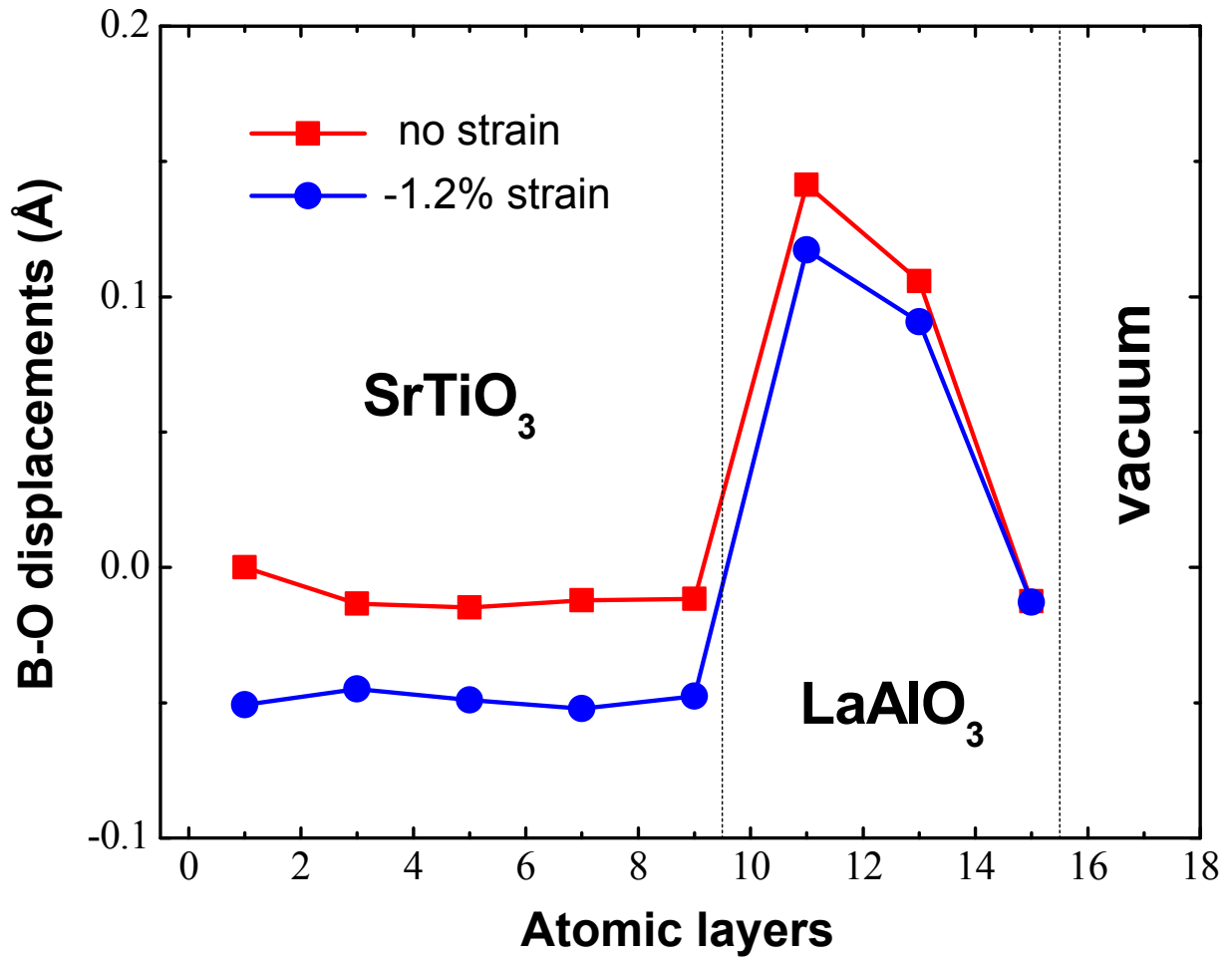


Figure 4, C.W. Bark et al

	a (Å)	c (Å)	bi-axial lattice mismatch
<i>LaAlO3 (10uc) on SrTiO3 (50uc) on NdGaO3</i>			
SrTiO3	3.860	3.964	-1.21%
NGO	3.859	3.866	
<i>LaAlO3 (10uc) on SrTiO3 (50uc) on LSAT</i>			
SrTiO3	3.868	3.940	-0.96%
LSAT	3.869	3.387	
<i>LaAlO3 (10uc) on SrTiO3 (120nm) on Si</i>			
SrTiO3	3.911	3.985	0.15%
Si	3.840	3.840	
<i>LaAlO3 (10uc) on SrTiO3 (20uc) on DyScO3</i>			
SrTiO3	3.944	3.939	1.11%
DyScO3	3.944	3.939	
<i>LaAlO3 (10uc) on SrTiO3 (20uc) on GdScO3</i>			
SrTiO3	3.964	3.875	1.59%
GdScO3	3.963	3.967	

Table 1. Bi- axial strain of SrTiO3 templates.